

Prediction of the Cutting Temperatures of Stainless Steel with Chamfered Main Cutting Edge Tools

Chung-Shin Chang

Department of Mechanical Engineering, National Ilan University, No. 1, Shen-Lung Rd., I-Lan, 26014, Taiwan, ROC

Abstract

The main purpose of this report is to predict the temperature of carbide tip's surface and study the cutting forces of turning stainless steel with sharp chamfered main cutting tools. The friction forces and frictional heat generated on elementary cutting tools are calculated by using the measured cutting forces and the oblique cutting analysis. The temperature of carbide tip surface is solved by finite element analysis (FEA) and compared with those obtained from experimental measurements. A good agreement demonstrates the accuracy of the proposed model.

Keywords :

Chamfered main cutting edge, FEM, stainless steel, temperature of stainless steel

1. INTRODUCTION

Cutting temperature is an important parameter in the analysis metal cutting process. Usui and Hirota [1, 2] used an iterative technique to find the chip flow direction minimizing the sum of the shear and friction energies. Singamneni [3] demonstrated the mixed finite and boundary element method finally enables the estimation of the cutting temperatures which is a simple, efficient method, and at the same time it is quite easy to implement. Chang and Fuh [4] presented a model to accurately predict the cutting force for turning of stainless steel with a chamfered main cutting edge sharp tool. The objective of this paper is to set up an oblique cutting stainless steel model to study three-dimensional cutting temperature for a sharp tool with a chamfered main cutting edge.

2. THEORETICAL ANALYSIS

In recent years, the finite element method has particularly become the main tool for simulating metal cutting processes [5]. The aim of this paper is to clarify the metal cutting temperature with the chamfered main cutting edge sharp tool of three-dimensional deformation. According to Chang and Fuh [4], a force model for turning of stainless steel with a chamfered main cutting edge, which can accurately predict the formations of shear planes for the case of chamfered main cutting edge, must have nose radius R , cutting depth d , feed rate f , cutting speed V , and parallel back rake angle α_b , C_s is the side cutting edge angle, C_e is the end cutting edge angle, α_{s1} is the first side rake angle, and α_{s2} is the second side rake angle. α_{s1} and α_{s2} are used as shown in figure 1 and Table 1.

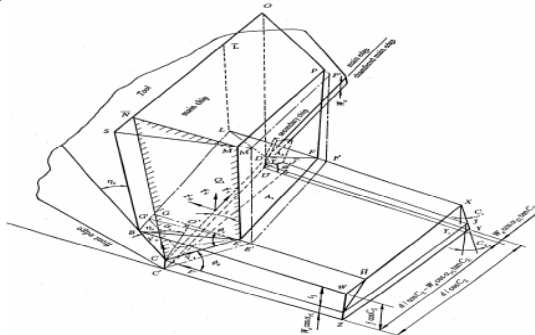


Figure 1 A force model of chamfered main cutting edge sharp tool ($R=0, f > R$)

Table 1 Tool geometries specifications

side cutting edge angle C_s	tool no.	side rake angles α_{s1}, α_{s2}	nose roundness (R)
20°	1	10°, -10°	0.0(unchamfered)
20°	2	10°, -10°	0.0(chamfered)
30°	3	10°, -10°	0.0(unchamfered)
30°	4	10°, -10°	0.0(chamfered)
40°	5	10°, -10°	0.0(unchamfered)
40°	6	10°, -10°	0.0(chamfered)
notation: tool holder and tips			

2.1 The shear areas in the cutting process for sharp tool

The shear plane area A includes the area of the triangle A_1 , trapezoid area of A_2 , and secondary chip's A_s , shown Fig. 1.

$$A = A_1 + A_2 + A_s \quad (1)$$

$$A_1 = \frac{t_3^2}{4 \cos^2 \alpha_{s2}} \left\{ \frac{4 \cos^2 \alpha_e}{\sin^2 \phi_e \cos^2 \eta_c} - \left[1 + \frac{\cos^2 \alpha_e}{\sin^2 \phi_e \cos^2 \eta_c} - (1/\cos^2 \eta_c) [\sin^2 \eta_c + (\sin \alpha_e + \cos \alpha_e \cot \phi_e)^2 - 2 \sin \eta_c \sin \alpha_b (\sin \alpha_e + \cos \alpha_e \cot \phi_e)] \right]^2 \right\}^{1/2} \quad (2)$$

$$A_2 = t_3 \left(\frac{2b}{\cos \alpha_b} - \frac{t_3 \tan \eta_c}{\cos \alpha_{s2}} \right) \times \left\{ \cos^2 \alpha_e - \sin^2 \phi_e [\sin \eta_c (\sin \alpha_e + \cos \alpha_e \cot \phi_e) \sin \alpha_b]^2 \right\}^{1/2} / 2 \sin \phi_e \cos \alpha_{s2} \cos \eta_c \quad (3)$$

$$A_s = (W_e \cos \alpha_{s1})^2 \tan C_s / 2 (\cos \alpha_b \sin \phi_e) \quad (4)$$

The area of the projected cross section Q is equal to $Q = Q_1 + Q_2 + Q_3$.

$$Q_1 = 0.5(b_2 + b)t_3 / [\cos \alpha_b \cos \alpha_{s2}] \quad (5); \quad Q_2 = t_2 b_2 / \cos \alpha_b \quad (6)$$

$$Q_3 = W_e^2 \cos \alpha_{s1} \tan C_s / 2 \cos \alpha_b \quad (7)$$

According to above investigations, the cutting force is a function of parameters $\alpha_{s1}, \alpha_{s2}, \alpha_b, d, W_e, \theta_{ref}, C_s, C_e, f, V,$ and η_c . Once η_c had been determined, $\alpha_e, \varphi_e, \tau_s$ and β that describe chip formation can be determined, figure 1. By changing the value of η_c in the developed computer program, the cutting force can be calculated. The calculation procedure for the cutting force and the inverse heat transfer solution are shown in figure 2.

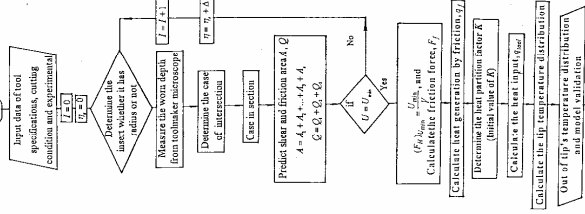


Figure 2 Flow chart of the cutting force and the inverse heat transfer solution

2.2 The energy method to predict cutting force

The shear energy per unit time (U_s) and the friction energy per unit time (U_f) were proposed by Usui [1] as:

$$U = U_s + U_f \quad (8), \quad U_s = F_s V_s = F_s V \cos \alpha_e / \cos(\varphi_e - \alpha_e) \quad (9)$$

$$U_f = F_t \cdot V_c = f_t \int_0^{B_1} db \cdot V_c = \frac{\tau_s \sin \beta \cos \alpha_e Q V}{[\cos(\phi_e + \beta - \alpha_e) \cdot \cos(\phi_e - \alpha_e)]} \quad (10)$$

where the symbol α_e represents the effective rake angle (rad), α_b denotes the back rake angle (rad), φ_e is the effective shear angle and equals $0.581\alpha_e - 1.139$ (rad), β is the friction angle (rad) which equals $\exp(0.848\alpha_e - 0.416)$ [2], τ_s is the shear stress which equals $571 - 19.9\alpha_e$ (MN/m^2) [4], C_s is the chip flow angle which is determined by minimizing the total cutting energy U and $\tau_s = \sigma_y / 2$, $\sigma_y = HB / \pi$.

$U_{\min} = V(F_H)_{U_{\min}}$ (11); where $U_{\min} = U_s + U_f$ (12) and F_H is the cutting force, and V is the cutting speed. Therefore,

$$F_H = (F_H)_{U_{\min}} = U_{\min} / V = \{ \tau_s \cos \alpha_e A / \cos(\varphi_e - \alpha_e) + \tau_s \sin \beta \cos \alpha_e Q / \cos(\phi_e + \beta - \alpha_e) \cos(\varphi_e - \alpha_e) \} \quad (13)$$

$$(R_t)_H = N_t \cos \alpha_{s2} \cos \alpha_b + (F_t)_{U_{\min}} \sin \alpha_e = (F_H)_{U_{\min}} \quad (14)$$

$$F_t = \tau_s \sin \beta \cos \alpha_e Q / [\cos(\varphi_e + \beta - \alpha_e) \sin \varphi_e] \quad (15)$$

$$N_t = [(F_H)_{U_{\min}} - (F_t)_{U_{\min}} \sin \alpha_e] / (\cos \alpha_{s2} \cos \alpha_b) \quad (16)$$

$$F_T = -N_t \cos \alpha_{s2} \sin \alpha_b + F_t (\sin \eta_c \cos \alpha_b - \cos \eta_c \sin \alpha_{s2} \sin \alpha_b) \quad (17)$$

$$F_V = -N_t \sin \alpha_{s2} + F_t \cos \eta_c \cos \alpha_{s2} \quad (18)$$

2.3 Solid model of carbide tip

The chamfered main cutting edge tool has more special geometry. The tip cross-section profiled perpendicular (TCSP) to the main cutting edge was measured using an optical tool maker microscope, then a CAD software, SolidWorksTM, was used to generate the tip body by sweeping the TCSP along the main cutting edge with the specified pitch. Finally the tip's main cutting edge was simulated to remove unwanted material and create the solid model of turning tip geometry, as shown in figure 3.

2.4 Finite element model

The finite element analysis software is used in this study. The finite element mesh of the carbide tip is shown in figure 3 which has modeled by 58,000 four-node tetrahedral elements. As shown in the figure 3, 8*6 nodes are located on the projected contact length between the tool (about 3.29mm) and the workpiece, 3*6 nodes are located on chamfered width (0.23mm) of main cutting edge, and 1*6 nodes are placed on flank wear (0.03mm). The initial condition of finite element analysis has uniform temperature of 25°C in the tip.

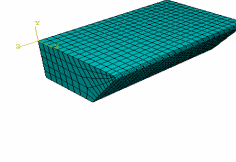


Figure 3 Finite element mesh of the chamfered main cutting edge tool

2.5 Modified carbide tip temperature model

Magnitude of tip's load is shown in following equations (19) and (20)

$$K = U_f / A' \quad (19); \quad A' = L_p (d + W_e + V_b) \quad (20)$$

A' is the area of friction force action, U_f is the friction energy, W_e is the tip's chamfered width, d is cutting depth, V_b is flank wear of tips and for simplification. L_f is the contact length between the cutting edge and the workpiece, L_p is the projected contact length between the tool and the workpiece, as referred to in figure 4, and can be determined according to the following conditions.

$$L_f = d / \cos C_s + f_1 \cos C_s / [\cos(C_e - C_s) \cos \alpha_{s2}] \quad (21)$$

$$L_p = d \sin C_s / \cos C_s + f_1 \cos C_s \cos C_e / [\cos \alpha_{s2} \cos(C_s - C_e)] \quad (22)$$

$$\rho c \partial T / \partial t = k \partial^2 T / \partial x^2 + k \partial^2 T / \partial y^2 + k \partial^2 T / \partial z^2 \quad (23); \quad q_{tool} = K q_f \quad (24)$$

where ρ is density, c is thermal conductivity, and k is heat capacity. The heat generation by assuming the cutting edge is perfectly sharp, the friction force, and chip velocity are multiplied to calculate the line heat generation rate, q_f , on cutting edge. $q_f = F_f V_c$. q_{tool} on each cutting edge is as above equation (24).

2.6 Inverse heat transfer solution and validation:

The flowchart for inverse heat transfer solution of K is summarized in figure 2. The AbaqusTM solver was used. By assuming a value for K , the spatial and temporal temperature distribution of the tip can be found. The discrepancy between the experimentally measured temperature at infrared pyrometer, j at time t_i , $T_j^i |_{\text{exp}}$ and finite element estimated temperature at the same infrared location and time, $T_j^i |_{\text{est}}$, determines the value of the objective function.

$$Obj(K) = \sum_{i=1}^{n_i} \sum_{j=1}^{n_j} (T_j^i |_{\text{exp}} - T_j^i |_{\text{est}})^2 \quad [5] \quad (25)$$

3. EXPERIMENTAL METHOD AND PROCEDURE

To verify the developed force and cutting temperature model, experimental arrangement is set up, as shown in figure 4. The workpieces are stainless steel, SUS304 65 mm diameter; 500 mm lengths cut from the same bar are used. The cutting tools

used in the experiments are Sandvik p10, S1P [6]. Tool composition: WC 69% , TiC 15% , TaC 8% , Co 8% , HV =1740 , density=10.3 g/cm³ , thermal conductivity =25W/m-°K and heat capacity= 210J/Kg-°K . The tool geometries are summarized in Table 1. The experimental tests are maintained at the same conditions as follows: dry cutting, cutting velocity: 45m/min; cutting depth: 2mm; feedrate:0.33mm/rev. The data are recorded three times at different sections. The average values will be taken.

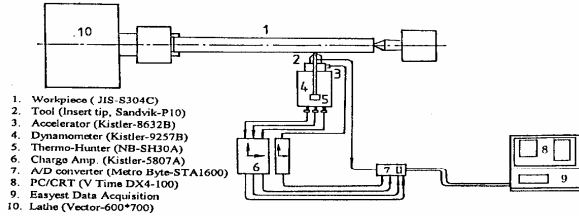


Fig. 4 Experimental set-up

4. RESULTS AND DISCUSSION

4.1 The Cutting Forces

According to the investigations under a constant side cutting edge angle C_s , Chang and Fuh [4] calculated that the increase of the side rake angles α_{s1} and α_{s2} results in the decrease of cutting force F_H and F_V . However, for C_s equals 20° , an increase of α_{s1} and α_{s2} , increased the cutting force F_T . The reason was that the contact length between the cutting edge of tool and the workpiece were increased.

4.2 Temperature of surface of tip

Inverse heat transfer utilizes the temperature measured by infrared on the surface of tip as the input to predict the heat flux on the chamfered main cutting edge tools.

- Based on Lin et al. [7], a finite element method with an inverse scheme and an experimental measurement using infrared detector was used to monitor the temperature at the tool-chip interface, and the temperature was also recorded by the computer. It can be concluded that the tip's surface temperature does not exceed 220°C as a sharp tool is used in turning carbon steel [8].
- Based on Li and Albert [5], according to equations (24) and (25), the flowchart for inverse heat transfer solution of K is summarized in figure 2. After finding the value of K , the finite element model can be applied to calculate temperature at tips, the results are shown in figures 5-8.

Figure 5 and 6 show the cutting temperatures vs. cutting time for different values α_{s1} and α_{s2} with chamfered and unchamfered sharp tool at d=2.0mm, f=0.33mm/rev, V=120m/min at $C_s = 20^\circ$ and $C_s = 30^\circ$ respectively. Figure 7 shows the cutting temperatures vs. C_s for different values α_{s1} and α_{s2} with chamfered and unchamfered sharp tool at d=2.0mm, f=. 33mm/rev, V=120m/min respectively. Figure 8 shows the cutting temperatures distribution with chamfered main cutting edge sharp tool at $C_s = 30^\circ$, $\alpha_{s1} = -30^\circ$ and $\alpha_{s2} = 30^\circ$, d=2.0mm, f=0.33mm/rev, and V=120 m/min.

- From figures 5-6, it proved that the cutting edge temperature of the chamfered main edge tool was lower than unchamfered main edge tool.

- According to figures 5-7, the tip temperatures of chamfered main cutting edge tool were very low and the inverse data correlates closely with the experimental values.
- From figure 8, it proved that the distribution of chamfered main cutting edge tool's temperature was close the figure 6.
- From figure 7, the cutting temperatures of chamfered main cutting edge tool is the lowest, when $C_s = 30^\circ$, $\alpha_{s1} = -30^\circ$ & $\alpha_{s2} = 30^\circ$, and the temperature is not exceed 390°C.

5. CONCLUSIONS

Good correlations between predicted values and experimental results of forces and temperatures during machining with sharp tools in cutting stainless steel. The new tool model with chamfered main cutting edge has been developed by including the variation of shear plane areas. In this model, the energy method is also used to accurately predict cutting force. The FEM and Inverse heat transfer solution in tool temperature in stainless turning is obtained and compared with experimental measurements. The good agreement demonstrates the accuracy of proposed model. This model can be extended to on-line control domain in addition to the factors of time and thermal effect. Further work will extend to the analysis of nose radius tools. The above results demonstrate that the predicted values matched with the experimental values very well. Additionally, the new tool-worn model from using the variation of shear areas that occur in tool wearing conditions can be applied to accurately predict the cutting forces and the temperature of tool tip surface.

REFERENCES

- Usui, E. and Hirota, A., 1978, Analytical Prediction of Three Dimensional Cutting Process, part 2, Chip Formation and Cutting Forces with Conventional Single-Point Tool, Trans. ASME, Journal of Engineering for Industry, 100:229-235
- Usui, E., Hirota, A. and Masuko, M., 1978, Analytical Prediction of Three Dimensional Cutting Process, part 1, Basic Cutting Model and Energy Approach, Trans., ASME, Journal of Engineering for Industry, 100: 222-228
- Singamneni, S. B., 2005, A Mixed Solution for Three-Dimensional Temperature Distribution in Turning Inserts Using Finite and Boundary Element Techniques, J. of Materials Processing Technology, 166: 98-106
- Chang, C. S. and Fuh, K.H, 1995, Turning of Stainless Steel with Chamfered Main Cutting Edge Tools, J. of Materials and Manufacturing Processes, 10:473-492
- Li, Rui and Shih, A. J., 2005, Inverse Heat Transfer Solution in Tool Temperature Titanium Drilling, Mechanical Engineering, University of Michigan Ann Arbor,
- Brookes, K. J. A., 1992, World Directory and Handbook of Hard Metals, 5th edition, published by International Carbide Data Hand book, United Kingdom: D172-175,
- Lin, J.M., Liu, C.Y., 2001, Measurement of Cutting Tool Temperature by an Infrared Pyrometer, Journal of Measurement Science and Technology, 12:1243-1249
- Chang, C. S. , 1995, Prediction of the Cutting Forces for Chamfered Main Cutting Edge Tools, Int. J. of Machine Tools, Manufacture, Design and Research, 35:1559-1586

ACKNOWLEDGMENTS:

This work was supported by National Science Council, Taiwan, R.O.C. under grant number NSC 94-2218-E-197-CC1-003

Appendix A: Coefficients of the sharp (R=0):

$t_1 = f \cos C_s$ (A1); $t_2 = W_e \cos \alpha_{s1}$ (A2); $t_3 = t_1 - t_2$

$f_1 = f - W_e \cos \alpha_{s1}$ (A4); $b = d / \cos C_s$ (A5)

(A3) $b_4 = t_2 \tan C_s$ (A6); $b_2 = b - b_4$ (A7)

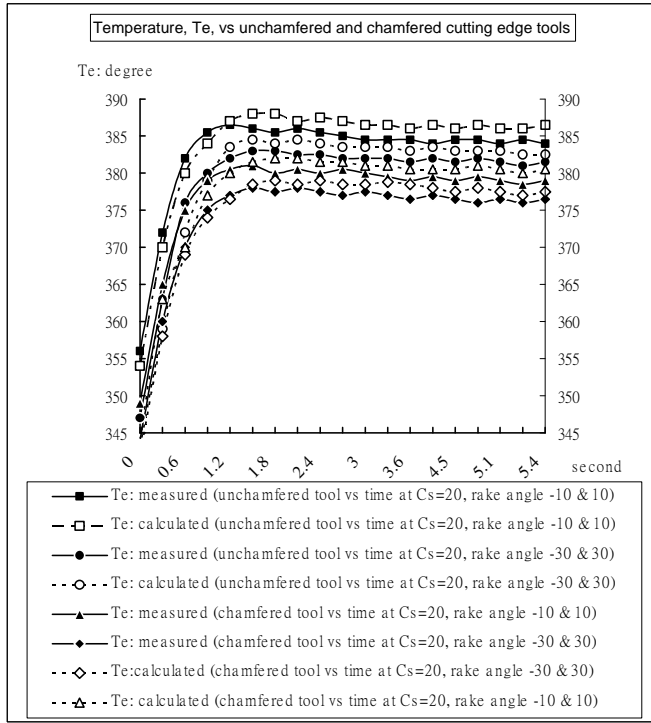


Figure 5 Cutting temperatures vs. cutting time for different values α_{s1} and α_{s2} with unchamfered and chamfered sharp tool at $d=2.0\text{mm}$, $f=0.33\text{mm/rev}$, $V=120\text{ m/min}$ and $C_s = 20^\circ$ (stainless steel)

tool at $d=2.0\text{mm}$, $f=0.33\text{mm/rev}$, $V=120\text{ m/min}$ and $C_s = 30^\circ$ (stainless steel)

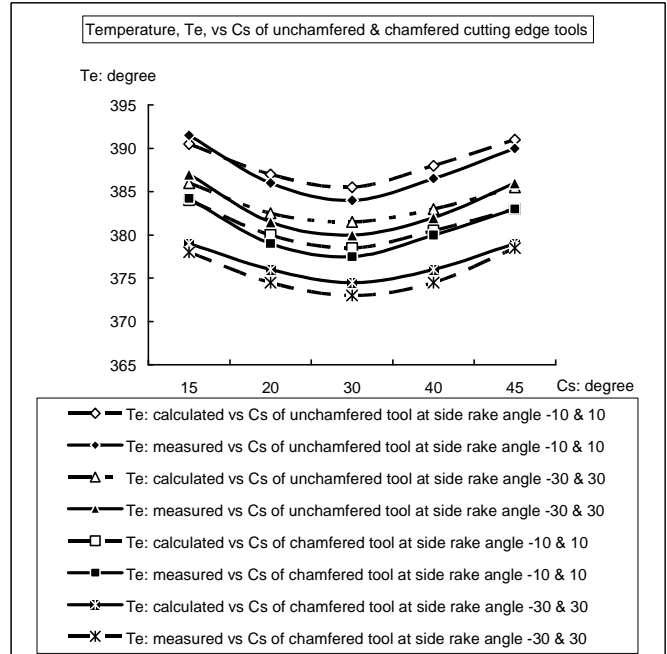


Figure 7 Cutting temperatures vs. C_s for different values α_{s1} and α_{s2} with unchamfered and chamfered sharp tool at $d=2.0\text{mm}$, $f=0.33\text{mm/rev}$, and $V=120\text{ m/min}$ (stainless steel)

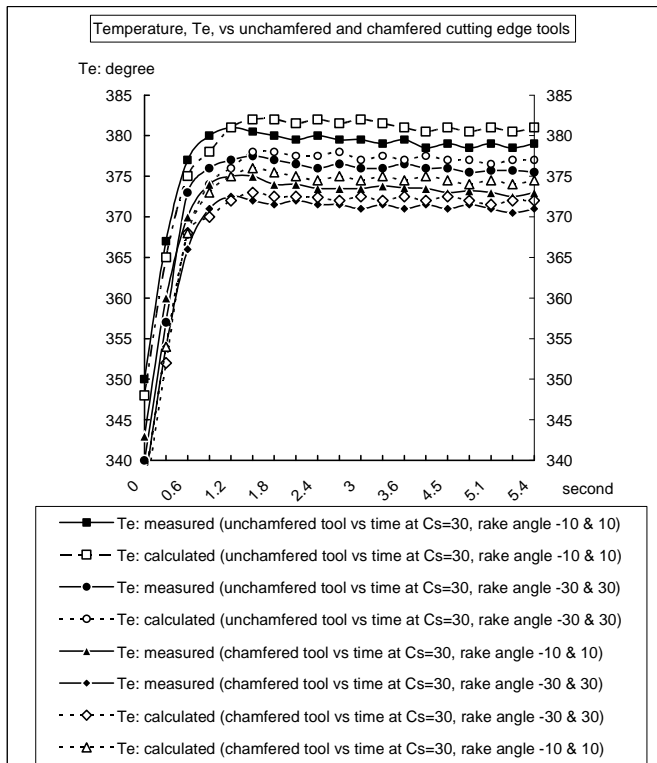


Figure 6 Cutting temperatures vs. cutting time for different values α_{s1} and α_{s2} with unchamfered and chamfered sharp

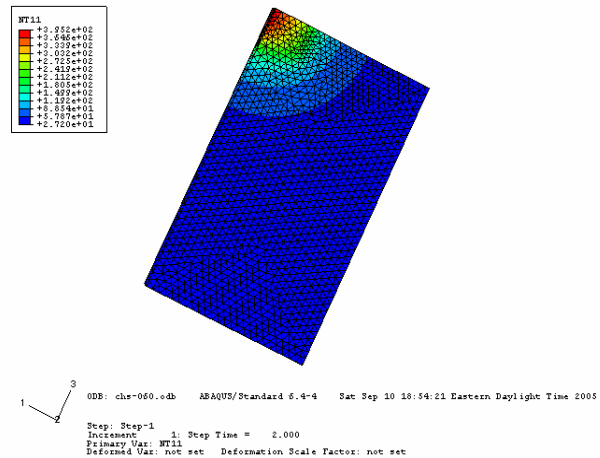


Fig. 8 Temperature distribution with chamfered cutting edge inserts near the tool nose at $C_s = 30^\circ$, $\alpha_{s1} = -30^\circ$ and $\alpha_{s2} = 30^\circ$, $d=2.0\text{mm}$, $f=0.33\text{mm/rev}$, and $V=120\text{ m/min}$ (stainless steel)